Available online at www.sciencedirect.com
SCIENCE DIRECT®
Materials Research Bulletin 39 (2004) 1299–1318
Materials Research Bulletin
www.elsevier.com/locate/matresbu

A new alternative representation of impedance data using the derivative of the tangent of the phase angle Application to the YSZ system and composites

Juan Carlos Ruiz-Morales[a], David Marrero-López[a], John T.S. Irvine[b], Pedro Núñez[a,*]

[a]*Department of Inorganic Chemistry, University of La Laguna, Canary Islands, Spain*
[b]*School of Chemistry, University of St. Andrews, Scotland, UK*

Received 11 February 2003; received in revised form 29 March 2004; accepted 31 March 2004

Abstract

The aim of this work is to propose a new alternative representation of impedance data using the derivative of the tangent of the phase angle, which allows enhanced discrimination between processes with relaxation frequencies that are very close. The new representation allows discrimination between overlapped processes within a factor of 2 in their relaxation frequencies for process with similar strength. Equations for the simplified behaviour of the impedance data have been proposed to obtain all the parameters of the processes involved in the impedance spectrum. This new alternative representation has been applied to bulk and grain boundary responses of YSZ with very satisfactory results. It has also been applied to the qualitative study of impedance data of a CuO composite showing the usefulness of this representation to discriminate different electrode processes. This approach provides an ab initio method of identify the contributing components to an electrochemical impedance spectrum with quite remarkable resolution. It is suggested that if this method is applied to provide starting parameters for non-linear least squares fitting using constant phase elements, then problems due to correlation of parameters and identification of components can be minimised.

Keywords: A. Ceramics; A. Composites; C. Impedance spectroscopy; D. Electrical properties

1. Introduction

Impedance spectroscopy EIS [1] is extensively used to study all type of processes, to resolve bulk and grain boundary contributions from the total conductivity of a material, interfacial kinetics in batteries

* Corresponding author. Tel.: +34-922-31-85-01; fax: +34-922-31-84-61.
E-mail address: pnunez@ull.es (P. Núñez).

0025-5408/$ – see front matter © 2004 Elsevier Ltd. All rights reserved.
doi:10.1016/j.materresbull.2004.03.026

and fuel cells, surface reactions and mass transport through porous electrodes in wet or dry conditions, polymer formation, to monitor the corrosion of metals in different environments or to study coating corrosion protective properties, etc.

Essentially, EIS involves applying a small, sinusoidal voltage or current signal to an electrochemical cell, measuring the system's response current or voltage, respectively with respect to amplitude and phase. The impedance of the system is determined by complex division of ac voltage by ac current. This process is performed for a certain range of frequencies for each sample. Finally, the parameters related with the macroscopic properties of these materials are obtained by fitting the impedance data to an equivalent circuit or model.

Among these materials, electroceramics are widely studied as materials for fuel cells, gas sensor or electrochemical applications. Their properties depend on the phase composition, sintering temperature, gas composition, impurities, etc. Their modification will affect the bulk and grain boundary transport properties, so a good understanding of these properties is necessary to develop new materials and to optimise the conductivity by control of crystal structure.

The equivalent circuit to study these ceramic materials often includes three components with their corresponding relaxation frequencies. At higher frequencies, the component normally corresponds to the bulk properties (f_b), at intermediate frequency the element corresponds to the grain boundaries (f_{gb}), and at low frequency, we usually have the electrode processes (f_{el}) or processes occurring at the material/electrode interface.

The values that characterise each process are easily obtained by fitting experimental data to equivalent circuits, if the relaxation frequencies of the different processes are well-resolved, usually $f_{el} \ll f_{gb} \ll f_b$, where b = bulk, gb = grain boundary and el = electrode. Typically, f_b is one or two orders of magnitude higher than f_{gb} and f_{el} is much smaller than f_{gb}. However, when overlapping between processes increases, equivalent circuit fitting can lead to wrong values. For this reason, different alternative representations have been used to solve the overlapped processes.

Abrantes et al. [2,3] demonstrate the ability of the representation of $\log(\tan(\delta))$ versus $\log(f)$ to reveal the bulk, grain boundary and electrode components of impedance spectra. At same time, they pointed out that the Z'' versus Z', $\log(Z'')$ versus $\log(f)$, $\log(M'')$ versus $\log(f)$ and $\log(A'')$ versus $\log(f)$ plots often have a limited applicability. All the contributions to the spectra are obtained from the minima and peaks of those plots.

West and co-workers [4,5] proposed a method based on combined spectroscopic plots of the imaginary components of impedance, Z'' and electric modulus M''. The method can be used to probe the electrical homogeneity of ceramics. The quantitative analysis of the spectra is obtained from the Debye peaks in the M'' and Z'' versus $\log(f)$ plots, due to the peaks in Z'' spectra being directly proportional to R and inversely proportional to C in the M'' spectra.

Another way is to use deconvolution methods. In the method used by Schichlein et al. [6,7], the distribution of relaxation times is computed directly from the experimental impedance data without any a priori assumptions about the internal structure of the system in the form of equivalent circuit models. The starting point is a model made by a serial connection of RC elements, then they assume an infinite number of elements with relaxation times ranging continuously from 0 to ∞ to obtain the convolution equation in accord with the Fuoss and Kirkwood treatment [8]. Since the real and imaginary part of the impedance are connected through the Kramers–Kronig transformations [9,10] only the imaginary parts were considered. After that, the data were logarithmically sampled and using the corresponding substitutions the convolution equation were obtained. A Fourier transformation was

applied to work in the transformed space, and then a Hanning filter was applied to avoid numerical error amplification. After filtering, inverse Fourier transformation gives the looked-for distribution function. In simulated cases, it is possible to resolve up to three physically distinct processes within one-decade frequency. Macdonald [11] obtained the distribution function of the relaxation frequencies using a weighted, non-linear least-squares inversion method, which avoids some of the inversion problems. The method was applied to dielectric data, but it can be applied to a conducting system or to inverse-diffusion problems. The dielectric response is expressed as a normalised frequency–response function and after the corresponding mathematical treatment the convolution equation is obtained.

An alternative method is the Differential Impedance Analysis (DIA) proposed by Raikova et al. [12]. DIA is a new structural approach for impedance data analysis that allows to extract the impedance model directly from the experimental data without any initial hypothesis about the system. The principle of the DIA is the frequency scanning local analysis using a model of a simple order inertial system, called local operating system (LOM). The model recognition is obtained by the temporal analysis of the LOM parameters estimates. If the LOM corresponds in a given frequency range to the nature of the impedance model, then the estimates tend to exhibit a constant behaviour in this frequency range, in other case the analysis gives frequency dispersion, that is a Constant Phase Element.

If a model is proposed by any of the methods above mentioned, the parameters can be obtained by a non-linear fitting method [13–17]. All of them generally use the algorithm developed by Levenberg [18] and Marquardt [19]. The convergence of the fitting depends of the starting values and it always is necessary to have an idea of the model, for this reason is the above mentioned representations or methods are needed. According to this, Boukamp [17] used a special subroutine in his software EQUIVALENT CIRCUIT (EQUIVCRT), to provide a ''rough'' deconvolution of the immittance spectra and from that a probable equivalent circuit and the corresponding starting values are obtained.

It would be ideal to use only one type of representation to obtain both qualitatively the number of processes and the parameters that characterise them or at least the relationships between these parameters that could be used with other non-linear fitting methods to refine the proposed circuit.

In this paper, we have taken the $\log(\tan(\delta))$ approach due to its good discrimination capability, and we have modified it to propose a new alternative representation of the impedance data, which allows discrimination between overlapped processes within a factor of 2 in their relaxation frequencies and can be used as a tool to qualitatively study the evolution of a system under certain experimental conditions. We present some examples related to solid oxide fuel cell technology; however, the treatment can be generally applied.

2. Experimental

2.1. YSZ pellet

Powders of Yttria-Stabilised Zirconia (YSZ) from Tosoh (8 mol Y_2O_3/ZrO_2) were hydrostatically pressed at 1 ton applied for 2 min. The pellet, with a diameter of 10 mm and a thickness of 1 mm, was sintered at 1400 °C for 12 h. The heating and cooling ramp rates were 5 °C/min.

The impedance measurements were performed with a FRA Solartron 1260, and a Potentiostat/Galvanostat, Solartron 1287, at zero applied voltage, with a 200 mV of ac perturbation. Measurements were carried out in the 2.5×10^5 to 0.1 Hz frequency domain.

2.2. CuO composite

A cermet was prepared by mixing, $Y_{0.15}Zr_{0.57}Ti_{0.13}Ce_{0.15}O_{1.925}$ (YZTC6) with CuO (Aldrich) in the weight ratio YZTC6:CuO = 40:60. The CuO has previously been dried at 500 °C for 2 h. The powder mixture was planetary ball milled in acetone for 1 h using a zirconia container with zirconia balls. Then, the powder was fired at 1000 °C, in air, for 24 h, and the purity was checked by powder X-ray diffraction. A slurry of this sample was prepared, mixing with a binder (Decoflux VB41). This slurry was used to paint two identical and symmetrical layers on each side of YSZ–20% Al_2O_3 electrolyte plates from CeramTec AG (Germany).

The symmetrical cell with an anode of area 0.95 cm^2, and about 125 μm thickness of the electrodes was sintered onto the 300 μm thick electrolyte at 1000 °C. The electrode material was coated with an organo-platinum paste on each face, dried at 100 °C for 1 h and fired at 1000 °C for 1 h.

The sample was mounted in a ''compression jig'' with Pt wire electrodes, in a horizontal tube furnace. Temperature dependent resistance corrections, as had previously been determined for the jig, were applied. Measurements were also corrected for lead inductance. The ac impedance measurements on symmetrical cells were performed sequentially in air and 5% hydrogen (wet), cooling back to 500 °C before changing atmosphere. For each temperature sufficient time was allowed to obtain thermal equilibrium and the reproducibility of the measurements.

The impedance measurements were performed with a Solartron 1260 Frequency Response Analyser, at OCV, with a 15 mV of ac perturbation. Measurements were carried out in the 1 MHz to 0.1 Hz frequency domain.

3. Theory, results and discussion

If the ceramic material has a behaviour given by the ''brickwork'' model (Fig. 1a), the classical representation of Bauerle [20] can be used, where each process can be assigned to a single RC circuit. A RC element is described by way of a resistance and a capacitance placed in parallel. When these processes are developed sequentially, many circuits RC are used as processes exist.

Thus, for an ideal behaviour of the ceramic material we can use the basic circuit shown in Fig. 1b. Depending on the sintering degree of the samples however, the grain boundary can sometimes disappear in well-sintered samples. On the other hand, a new arc will appear if we have a non-conducting second phase in the grain boundary that partially blocks the ionic conduction. This arc is usually called a ''constriction arc''. For this reason, the equivalent circuit must be appropriately modified to introduce this new arc. The assignment of arcs to one or another process type depends upon the capacitive values [4,21] (Table 1).

Keeping in mind that the impedance of any arc RC is given by:

$$Z_{RC} = \frac{R_i}{1 + (f/f_i)^2} - \frac{(f/f_i)R_i}{1 + (f/f_i)^2} j$$

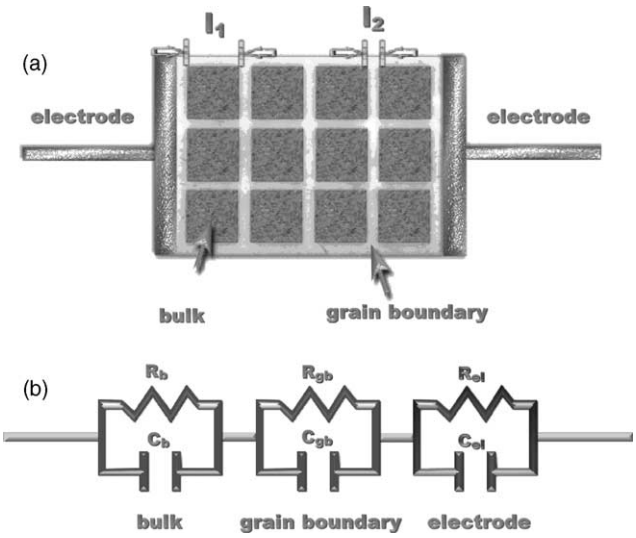

Fig. 1. Brickwork model of a ceramic material (a). Equivalent circuit model with RC elements in series (b).

where, i corresponds to the coefficient assigned to each processes, R is the resistance, f is the frequency and $j = \sqrt{-1}$. In accordance with the sequential development of the processes, the value of the global impedance, Z^*, is given by: $Z^* = Z' - jZ''$ (note that Z'' has to be a positive number in this equation), where

$$Z' = \frac{R_b}{1 + (f/f_b)^2} + \frac{R_{gb}}{1 + (f/f_{gb})^2} + \frac{R_{el}}{1 + (f/f_{el})^2} \quad \text{and}$$

$$Z'' = \frac{(f/f_b)R_b}{1 + (f/f_b)^2} + \frac{(f/f_{gb})R_{gb}}{1 + (f/f_{gb})^2} + \frac{(f/f_{el})R_{el}}{1 + (f/f_{el})^2}$$

If we make the logarithm of the quotient of real and imaginary part, we will obtain a function that we call $L(\theta)$, that is:

$$L(\theta) = \log\left(\frac{Z'}{Z''}\right) = \log\left\{\frac{[R_b/(1 + (f/f_b)^2)] + [R_{gb}/(1 + (f/f_{gb})^2)] + [R_{el}/(1 + (f/f_{el})^2)]}{[(f/f_b)R_b/(1 + (f/f_b)^2)] + [(f/f_{gb})R_{gb}/(1 + (f/f_{gb})^2)] + [(f/f_{el})R_{el}/(1 + (f/f_{el})^2)]}\right\} \quad (1)$$

Table 1
Typical capacitance values for some processes [4] using 1 cm^{-1} of geometrical factor (l/A) as reference

Process	Capacitance (F)
Bulk	10^{-12}
Minor, second phase	10^{-11}
Grain boundary	10^{-11} to 10^{-8}
Sample/electrode interface	10^{-7} to 10^{-5}
Electrochemical reactions	10^{-4}

Table 2
Theoretical values used for the simulated cases 1, 2 and 3. In all the cases the resistance of each process was $10^3\ \Omega$

Process	Case 1		Case 2		Case 3	
	$-\log C_i$ (F)	f_i (Hz)	$-\log C_i$ (F)	f_i (Hz)	$-\log C_i$ (F)	f_i (Hz)
Bulk	9.497	5×10^5	8.497	5×10^4	8.497	5×10^4
Grain boundary	7.497	5×10^3	7.497	5×10^3	8.196	2.5×10^4
Electrode	5.497	5×10^1	6.497	5×10^2	1.799	1×10^{-2}

where, $f_i = \omega_i/2\pi$, $\omega_i = 1/R_iC_i$, $\tau_i = R_iC_i$, f is the relaxation frequency, ω is the angular frequency, τ is the relaxation time or time constant and C_i is the capacitance of each process. $L(\theta)$ can be related with $\tan(\theta)$ through expression: $L(\theta) = \log(Z'/Z'') = -\log(-\tan(\theta))$, θ being the angle formed by Z' and Z''.

We will study the behaviour of the function $L(\theta)$ versus $\log(f)$. In case 1, the frequency of the processes (bulk, grain boundary and electrode) will differ by a factor of 10^2 while in case 2 by 10^1. In case 3 the frequency of the grain boundary process is only half of that of the bulk process.

3.1. Case 1

This shows the typical behaviour of this function with frequency, using a hypothetical case in which the processes are quite separate (Table 2, case 1).

Fig. 2 shows three different formalisms: (a) typical plot of Z'' versus Z'; (b) $|Z|$ and θ versus frequency; and (c) the plot of $L(\theta)$ versus $\log(f)$, for this case. Three processes can clearly be deduced from each plot.

A qualitative analysis of the $L(\theta)$ versus $\log(f)$ plot (Fig. 2c) shows that it is possible to observe zones corresponding to straight line of slope -1, these are the RC arc domain zones. If we had only one arc, we should only obtain one straight line with slope -1. In this sense, for each RC arc a straight line with slope -1 will be obtained.

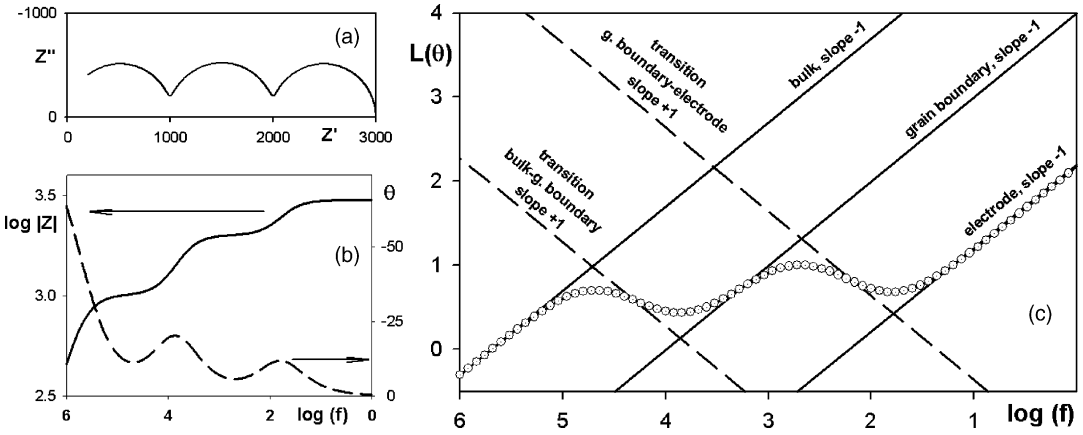

Fig. 2. Impedance spectra computed for $R_b = R_{gb} = R_{el} = 10^3\ \Omega$, $f_b = 5 \times 10^5$ Hz, $f_{gb} = 5 \times 10^3$ Hz, $f_{el} = 5 \times 10^1$ Hz. Nyquist plot (a), the corresponding plots of magnitude, $|Z|$ and phase angle, θ, vs. frequency (b), and $L(\theta)$ vs. $\log(f)$ (c).

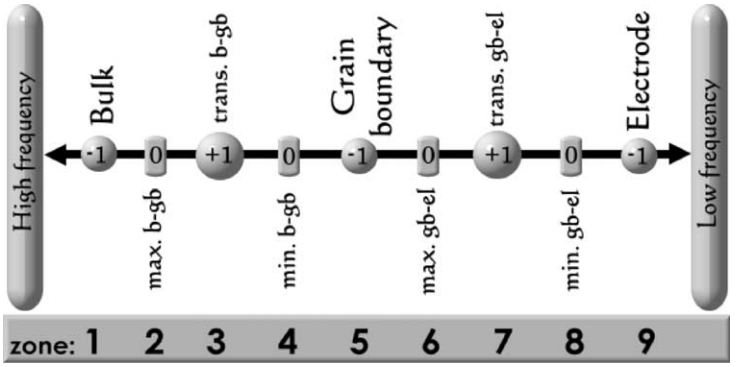

Fig. 3. Schematic representation of the frequency domain of each process, with the corresponding slope −1, +1 and 0.

In the transitions between the different arcs a change in the slope from −1 to +1 is observed when we decrease the frequency, in a well-resolved spectrum.

Evidently, in the transition zones between two straight lines of slope −1 (2 RC arcs) a maximum and a minimum will exist, so the slope of $L(\theta)$ versus $\log(f)$ must be zero in these points.

The frequency domains for each of the previously commented zone are shown in Fig. 3. The zones with even numbers (2, 4, 6 and 8) correspond to those with slope = 0; and lead to maxima (zones 2 and 6) and minima (zones 4 and 8) of $L(\theta)$. While zones with slope = −1 (1, 5 and 9) correspond to the bulk, grain boundary and electrode processes; and zones with slope = +1 (zones 3 and 7) correspond to transition zones.

Once the function $L(\theta)$ is qualitatively characterised we must obtain the equations corresponding to each zone.

First, we will consider zones with slope −1, where we can observe three cases: high, intermediate and low frequency (points (a)–(c)). Then we will take into account zones with slope +1, where two cases can be observed: bulk-grain boundary and grain boundary-electrode transitions frequency (points (d) and (e)). Finally, we will bear in mind zones (slope = 0) with maxima and minima of the function $L(\theta)$ (points (f)–(i)).

(a) *Straight line with slope −1, high frequency.*

In the zones with slope −1, and at higher frequency (Fig. 3, zone 1), only the bulk contribution will exist, and Eq. (1) can be simplified to:

$$L(\theta) \approx \log\left(\frac{R_b}{R_b/f_b}\right) - \log f \Rightarrow L(\theta) = \log[f_b] - \log f \tag{2}$$

(b) *Straight line with slope −1, intermediate frequency.*

In this case we will work in the frequency range corresponding to the zone 5 in Fig. 3, so $f \ll f_b$, $f \gg f_{el}$, where the electrode contribution is negligible, and moreover $f < f_{gb}$, so Eq. (1) will be reduced to:

$$L(\theta) \approx \log\left\{\frac{R_b + [R_{gb}/(1 + (f/f_{gb})^2)]}{(f/f_b)R_b + [(f/f_{gb})R_{gb}/(1 + (f/f_{gb})^2)]}\right\} \Rightarrow L(\theta) = \log\left[\frac{R_b + R_{gb}}{(R_b/f_b) + (R_{gb}/f_{gb})}\right] - \log f \tag{3}$$

(c) *Straight line with slope −1, low frequency.*

In this situation the frequency range corresponds to the zone 9 in Fig. 3, so $f \ll f_b$, $f \ll f_{gb}$ and $f < f_{el}$, therefore Eq. (1) can be written as:

$$L(\theta) \approx \log\left\{\frac{R_b + R_{gb} + [R_{el}/(1+(f/f_{el})^2)]}{(f/f_b)R_b + (f/f_{gb})R_{gb} + [(f/f_{el})R_{el}/(1+(f/f_{el})^2)]}\right\}$$

$$\Rightarrow L(\theta) = \log\left[\frac{R_b + R_{gb} + R_{el}}{(R_b/f_b) + (R_{gb}/f_{gb}) + (R_{el}/f_{el})}\right] - \log f \tag{4}$$

(d) *Straight line with slope +1, transition bulk-grain boundary.*

This transition corresponds to the zone 3 (Fig. 3), so $f > f_{gb}$, $f < f_b$ and $f \gg f_{el}$, consequently:

$$L(\theta) \approx \log\left[\frac{R_b + (R_{gb}/(f/f_{gb})^2)}{(f/f_b)R_b + ((f/f_{gb})R_{gb}/(f/f_{gb})^2)}\right] \Rightarrow L(\theta) = \log\left[\frac{R_b}{R_{gb}}\frac{1}{f_{gb}}\right] + \log f \tag{5}$$

(e) *Straight line with slope +1, transition grain boundary-electrode.*

This transition corresponds to the zone 7 (Fig. 3), so $f \ll f_b$, $f < f_{gb}$ and $f > f_{el}$, thus:

$$L(\theta) \approx \log\left[\frac{R_b + R_{gb} + (R_{el}/(f/f_{el})^2)}{(f/f_b)R_b + (f/f_{gb})R_{gb} + [(f/f_{el})R_{el}/(f/f_{el})^2]}\right] \Rightarrow L(\theta) = \log\left[\frac{R_b + R_{gb}}{R_{el}}\frac{1}{f_{el}}\right] + \log f \tag{6}$$

(f) *Maximum between bulk-grain boundary, slope 0.*

This maximum (zone 2) between the bulk and the grain boundary simply corresponds to the intercept between the straight line of slope −1 corresponding to the bulk process (Eq. (2)) with the straight line of slope +1 corresponding to the bulk-grain boundary transition (Eq. (5)). In consequence balancing both equations:

$$\log[f_b] - \log(f_{b\leftrightarrow gb}^{max}) = \log\left[\frac{R_b}{R_{gb}}\frac{1}{f_{gb}}\right] + \log(f_{b\leftrightarrow gb}^{max}) \Rightarrow \log(f_{b\leftrightarrow gb}^{max}) = \frac{1}{2}\log\left[f_b f_{gb}\frac{R_{gb}}{R_b}\right] \tag{7}$$

where, $\log(f_{b\leftrightarrow gb}^{max})$ is the frequency in which the maximum is reached in this region.

(g) *Minimum between bulk-grain boundary, slope 0.*

Analogously, the minimum (zone 4) between the bulk and the grain boundary corresponds to the intercept between the straight line of slope +1 corresponding to the bulk-grain boundary transition Eq. (5) with the straight line of slope −1 corresponding to the grain boundary process Eq. (3). So balancing both equations:

$$\log\left[\frac{R_b}{R_{gb}}\frac{1}{f_{gb}}\right] + \log(f_{b\leftrightarrow gb}^{min}) = \log\left[\frac{R_b + R_{gb}}{(R_b/f_b) + (R_{gb}/f_{gb})}\right] - \log(f_{b\leftrightarrow gb}^{min})$$

$$\Rightarrow \log(f_{b\leftrightarrow gb}^{min}) = \frac{1}{2}\log\left[\frac{R_{gb}}{R_b}f_{gb}\left(\frac{R_b + R_{gb}}{(R_b/f_b) + (R_{gb}/f_{gb})}\right)\right] \tag{8}$$

where, $\log(f_{b\leftrightarrow gb}^{min})$ is the frequency in which the minimum is reached in this region.

(h) *Maximum between grain boundary-electrode, slope 0.*

To obtain the theoretical equation corresponding to the maximum (zone 6) between the grain boundary and the electrode process, we should just find the frequency in which the straight line

with slope −1 (grain boundary, Eq. (3)) intercepts with the straight line of slope +1 (grain boundary-electrode transition, Eq. (6)), thus balancing both equations we will obtain:

$$\log\left[\frac{R_b + R_{gb}}{(R_b/f_b) + (R_{gb}/f_{gb})}\right] - \log(f^{max}_{gb\leftrightarrow el}) = \log\left[\frac{R_b + R_{gb}}{R_{el}}\frac{1}{f_{el}}\right] + \log(f^{max}_{gb\leftrightarrow el})$$

$$\Rightarrow \log(f^{max}_{gb\leftrightarrow el}) = \frac{1}{2}\log\left[f_{el}\frac{R_{el}}{(R_b/f_b) + (R_{gb}/f_{gb})}\right] \quad (9)$$

where, $\log(f^{max}_{gb\leftrightarrow el})$ is the frequency in which the maximum is reached in this region.

(i) *Minimum between grain boundary-electrode, slope 0.*

Finally, balancing Eq. (6), corresponding to the transition grain boundary-electrode, slope +1, with Eq. (4), corresponding to the electrode process, slope −1, the frequency of the minimum will be obtained, thus:

$$\log\left[\frac{R_b + R_{gb}}{R_{el}}\frac{1}{f_{el}}\right] + \log(f^{min}_{gb\leftrightarrow el}) = \log\left[\frac{R_b + R_{gb} + R_{el}}{(R_b/f_b) + (R_{gb}/f_{gb}) + (R_{el}/f_{el})}\right] - \log(f^{min}_{gb\leftrightarrow el})$$

$$\Rightarrow \log(f^{min}_{gb\leftrightarrow el}) = \frac{1}{2}\log\left[\frac{R_b + R_{gb} + R_{el}}{R_b + R_{gb}}\frac{R_{el}f_{el}}{(R_b/f_b) + (R_{gb}/f_{gb}) + (R_{el}/f_{el})}\right] \quad (10)$$

where, $\log(f^{min}_{gb\leftrightarrow el})$ is the frequency in which the minimum is reached in this region.

Thus, all the equations corresponding to the behaviour of the $L(\theta)$ function with the frequency have been deduced, in such a way that from these equations or together with the use of the classic representation of the magnitude $|Z|$ versus frequency is possible to determine the six parameters that characterise the three RC processes.

Obviously, all these equations can be simplified depending on the resistive values and the relaxation frequencies.

As the relaxation frequencies of the different processes reach similar values, the corresponding RC arcs are overlapped, so the problem is to obtain reliably the parameters of these arcs. This overlapping will also be reflected in the representation of $L(\theta)$ versus $\log(f)$, because each RC arc corresponds to a zone with straight line with slope −1. It is evident that if the relaxation frequencies are identical, it would not be possible to observe the different processes RC and we will only be able to see a straight line with slope −1. But, if the processes have slightly different relaxation frequencies it will be possible to obtain a sensitive representation to the transition between these processes.

The change of slope of the function $L(\theta)$ will perfectly reproduce any transition type, although the capability to discriminate processes with close relaxation frequencies will depend fundamentally on the dispersion of the experimental data and the number of points.

In order to be able to calculate the slope in each zone of the function $L(\theta)$ we will use the well-known numeric approach:

$$\text{slope} = \frac{dL(\theta)}{d\log(f)} \approx \left(\frac{\Delta L(\theta)}{\Delta\log(f)}\right)_{\Delta\log(f)\to 0} \quad (11)$$

The value of the slope will be obtained with great accuracy when small increments of $\log(f)$ are used. In general, very good values of the slope can be obtained using about 12 points per decade of frequency.

The plot of slope of $L(\theta)$ versus $\log(f_{mean})$ is built up by applying Eq. (11) to each pair of consecutive points. From Fig. 4a we can observe two zones with slope −1, at high and low frequencies, and another

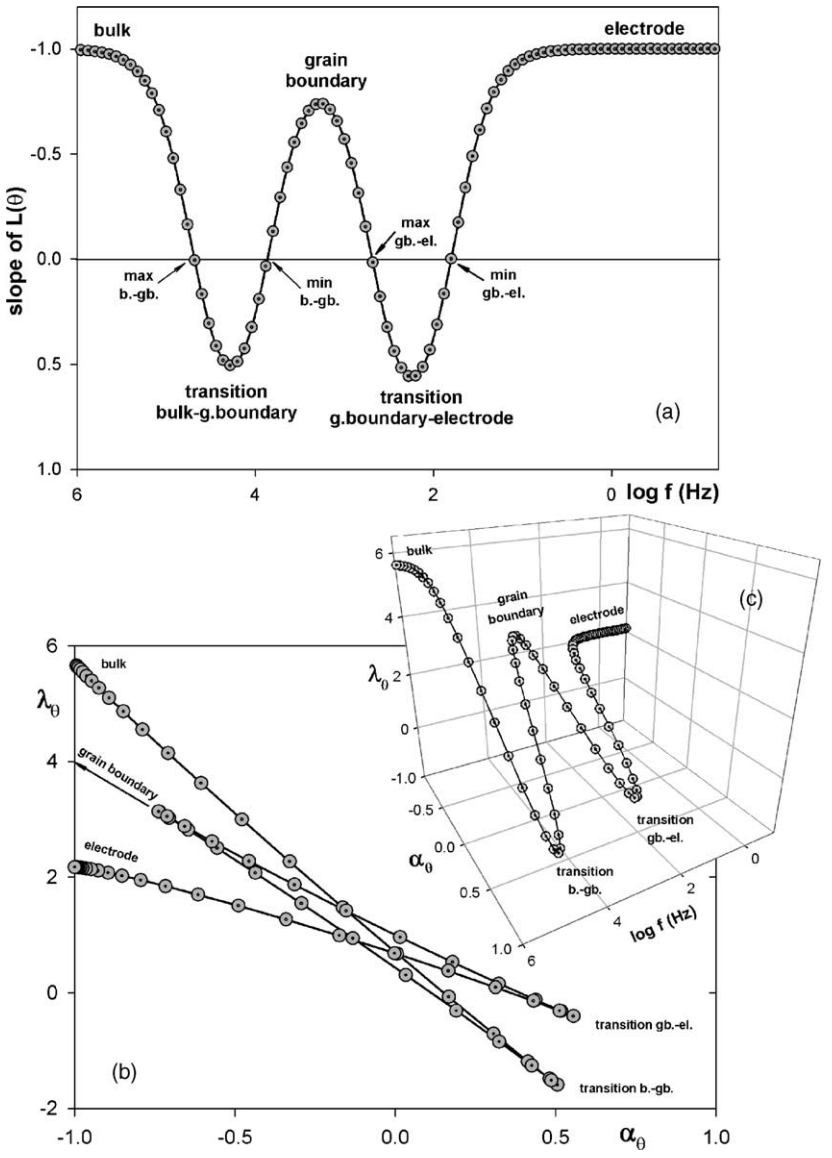

Fig. 4. Slope of the function $L(\theta)$ vs. frequency (a), intercept (λ_θ) vs. slope (α_θ) of the function $L(\theta)$ (b) and the corresponding 3D plot (c), computed for $R_b = R_{gb} = R_{el} = 10^3\ \Omega$, $f_b = 5 \times 10^5$ Hz, $f_{gb} = 5 \times 10^3$ Hz and $f_{el} = 5 \times 10^1$ Hz.

zone corresponding to the grain boundary process, at $\log(f) \cong 3.7$, whose slope approaches at -1. Similarly, two transition zones are observed at $\log(f) \cong 4.2$ and $\log(f) \cong 2.2$.

On the other hand, solving the following equation for each couple of points it is also possible to find the intercept corresponding to the straight line that goes through them.

$$L(\theta)_i = (\alpha_\theta)_i \log(f_i) + (\lambda_\theta)_i \tag{12}$$

where α_θ and λ_θ are the straight line parameters.

Fig. 4b shows a plot of the intercepts of $L(\theta)$ versus slope of $L(\theta)$, that is λ_θ versus α_θ. If the slope obtained coincides with -1, 0 or -1, the corresponding intercepts should coincide with the theoretical intercept deduced (Eqs. (2)–(10)).

Thus, the new alternative representation of the impedance data that we propose consists of the representation of calculated intercepts, λ_θ versus slopes of the function $L(\theta)$, α_θ.

The advantages of this new type of representation can be shown from Fig. 4b. Firstly, this representation is very sensitive to processes with small separations in its relaxation frequencies, as we will see later on.

In second place, from the extrapolations or intercepts to slope -1, 0 and $+1$, it is possible to apply all the deduced Eqs. (2)–(10) and to obtain the parameters or combinations of these, of the processes studied. For the case described in Fig. 4b, it is observed that the bulk and electrode processes are well-resolved, with numerous data that present slope -1, so Eqs. (2) and (4) can be applied to these data, respectively. For the grain boundary, which presents a slight overlapping, we can make an extrapolation of the data and then apply Eq. (3). The successive intercepts with the value of the slope 0 allow us to apply Eqs. (7)–(10). Finally, extrapolating to slope $+1$, the intercept values are obtained that allow us to apply Eqs. (5) and (6), for the transitions of bulk-grain boundary and grain boundary-electrode, respectively.

In spite of the advantages of this type of representation, it is not an explicit function of the frequency, given that we are plotting slopes versus intercepts and sometimes the plots can be overlapped. For this reason, we introduce the use of the 3D representation of the proposed function, using the frequency explicitly, because although the processes have the same intercepts, each one corresponds to different processes that take place in different frequency ranges, so it will be possible to easily discriminate the involved processes. This type of 3D representation for case 1 is shown in Fig. 4c. The same conclusion can be observed as from Fig. 4b; but it is also possible to determine qualitatively the frequency domain of each arc. It can clearly be verified that this 3D representation is equivalent to Fig. 4a and b.

Table 3 (case 1) shows the theoretical values of the intercept corresponding to Eqs. (2)–(10) and the values obtained from Fig. 4b, by extrapolation or intercepts points. It can be confirmed the perfect agreement between the theoretical data and those obtained of the intercepts and extrapolations to slopes -1, 0, $+1$ (Fig. 4b).

Table 3
Theoretical and extrapolated values, simulated cases 1 to 3 using the parameters from Table 2

Eq. no.	Slope	Case 1 (theoretical/experimental)	Case 2 (theoretical/experimental)	Case 3 (theoretical/experimental)	Case 4: YSZ (theoretical/experimental)
2	−1	5.70/5.69	4.70/4.66	4.70/4.62	5.57/5.57
3	−1	4.00/4.00	3.96/3.91	4.52/4.52	3.85/3.85
4	−1	2.17/2.17	3.13/3.13	−1.52/−1.23	0.0366/0.0366
5	+1	−3.70/−3.72	−3.70/−3.76	−4.40/−4.44	−2.61/−2.52
6	+1	−1.40/−1.40	−2.40/−2.41	2.30/2.30	−0.396/−0.468
7	0	4.70/4.68	4.20/4.02	4.55/4.52	3.99/4.04
8	0	3.85/3.86	3.83/4.02	4.46/4.52	3.25/3.18
9	0	2.70/2.69	3.18/3.02	1.11/1.07	2.19/2.16
10	0	1.79/1.80	2.76/3.02	−1.91/−1.91	−0.591/0.233

Experimental values obtained for YSZ pellet, at 325 °C, sintered at 1440 °C for 12 h, corresponding to the case 4.

Thus, it has been proven with a practical case that when the processes are well-resolved, the classic and the new proposed representations allow us to obtain the parameters of the analysed processes. But let us to see now what happens when these processes shows some more overlapping.

3.2. Case 2

In this case we simulate processes whose relaxation frequencies are only separated by one order in logarithmic scale, as listed in (Table 2, case 2).

The existence of three processes can be verified from the typical representations (Fig. 5a and b) or from the $L(\theta)$ function (Fig. 5c). The three processes are partially overlapped, but the grain boundary is the process with the biggest degree of overlapping.

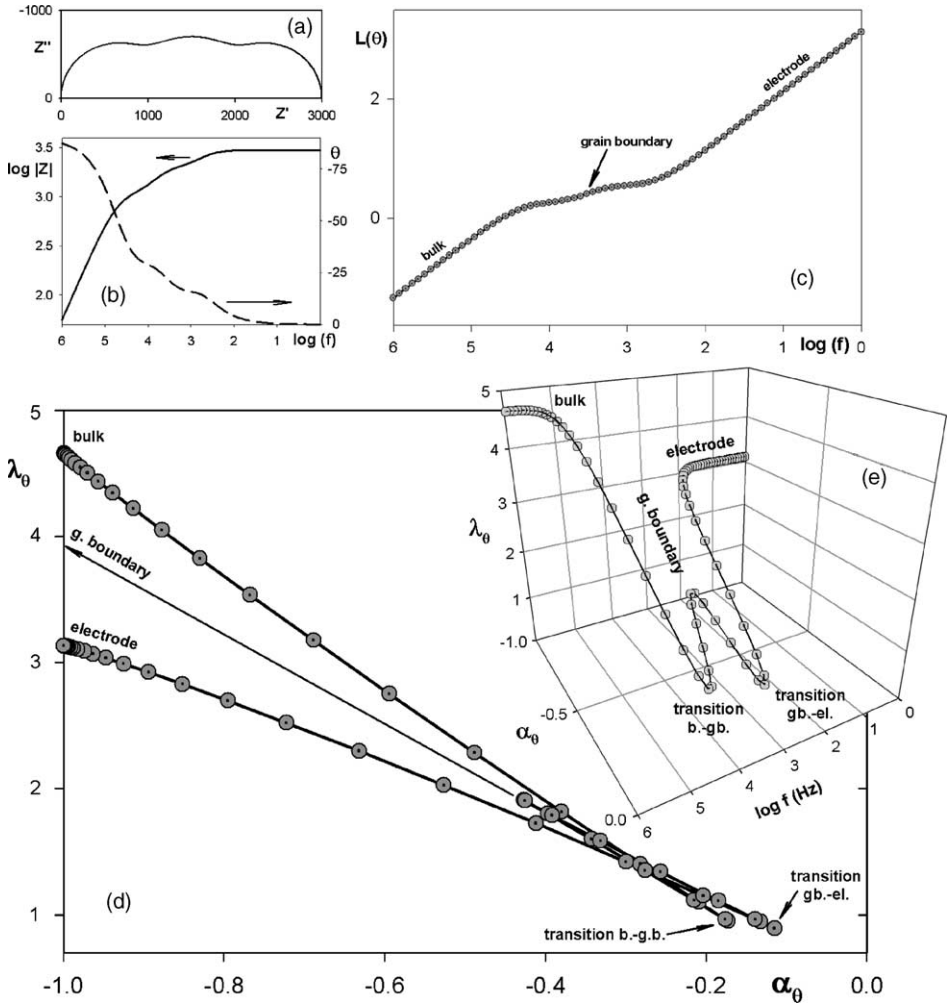

Fig. 5. Impedance spectra computed for $R_b = R_{gb} = R_{el} = 10^3\ \Omega$, $f_b = 5 \times 10^4$ Hz, $f_{gb} = 5 \times 10^3$ Hz and $f_{el} = 5 \times 10^2$ Hz. Nyquist plot (a), the corresponding plots of magnitude, $|Z|$ and phase angle, θ, vs. frequency (b), $L(\theta)$ vs. $\log(f)$ (c), and the new alternative representation of the impedance data in 2D (d) and 3D (e).

The new alternative representation, in 2D and 3D, for case 2 is shown in Fig. 5d and e. In this case, as we previously commented, the grain boundary presents a high degree of overlapping with the other processes (Fig. 5d). However, using the 3D representation (Fig. 5e), it can be clearly verified the existence of the three processes, and by extrapolations and intercepts points it will be possible to obtain the values shown in the (Table 3, case 2). From this table, the excellent agreement between the theoretical data and the data obtained by the new alternative representation can be confirmed.

In this case, the high overlapping rate of the grain boundary with the adjacent processes (Fig. 5b) does not allow us to clearly observe the maxima and minima that exists after and before the grain boundary. However, a slope change will exist between each one of these maximum–minimum, whose frequency range will correspond approximately with the half value of these maximum–minimum. Thus, for the maximum–minimum between the bulk-grain boundary, the theoretical values are:

$$\log(f^{\max}_{\mathrm{b}\leftrightarrow\mathrm{gb}}) = 4.20 \quad \text{and} \quad \log(f^{\min}_{\mathrm{b}\leftrightarrow\mathrm{gb}}) = 3.83$$

The mean value will be 4.02 and the value obtained by extrapolation (Table 3, case 2) is 4.02. For the maximum–minimum between the grain boundary-electrode, the theoretical values are:

$$\log(f^{\max}_{\mathrm{gb}\leftrightarrow\mathrm{el}}) = 3.18 \quad \text{and} \quad \log(f^{\min}_{\mathrm{gb}\leftrightarrow\mathrm{el}}) = 2.76$$

Obtaining a mean value of 2.97, also in very good agreement with the value obtained 3.02.

3.3. Case 3

Now, let us to suppose a extreme case, with two processes overlapped, the bulk and the grain boundary. With both processes overlapped within a factor of 2 in their relaxation frequencies, and with a well-resolved process corresponding to the electrode, as often happens in the reality for many ceramic materials under certain experimental conditions (see Table 2, case 3).

Usually, from the Nyquist and Bode plots (Fig. 6a and b) it will only possible to confirm the existence of 2 RC arcs, and the same conclusion can be obtained from the Fig. 6c. From this figure is possible to view a slight transition between the bulk and the grain boundary, however, using the new representation it will be possible to observe the existence of three processes clearly, and to obtain approximate relationships for the studied parameters.

Electric modulus would also show this with the smallest capacitance element dominating [4], however, unlike this formalism overlapping responses not involving the smallest capacitance element could not be resolving using modulus spectroscopy.

Fig. 6d and e shows the new representation in 2D and 3D where it is possible to observe the three processes and the overlapping ratio for the bulk with the grain boundary. Although the separation of the relaxation frequencies is only 0.3 units (in logarithmic scale), two processes can be clearly seen by magnification of domain area of the bulk and grain boundary (inset of Fig. 6d). The 3D representation (Fig. 6e) confirms with more clarity the existence of three processes not two.

The usefulness of this new representation to find relationships between the different parameters is again verified. In this case, the bulk and the grain boundary overlap does not allow us to observe the maximum and the minimum corresponding to this transition, but the transition should occur at intermediate value between this maximum–minimum. The theoretical values are 4.55 for the maximum and 4.46 for the minimum, and the mean value is 4.51. This value (4.52) fully agrees with the one obtained from the Fig. 6d.

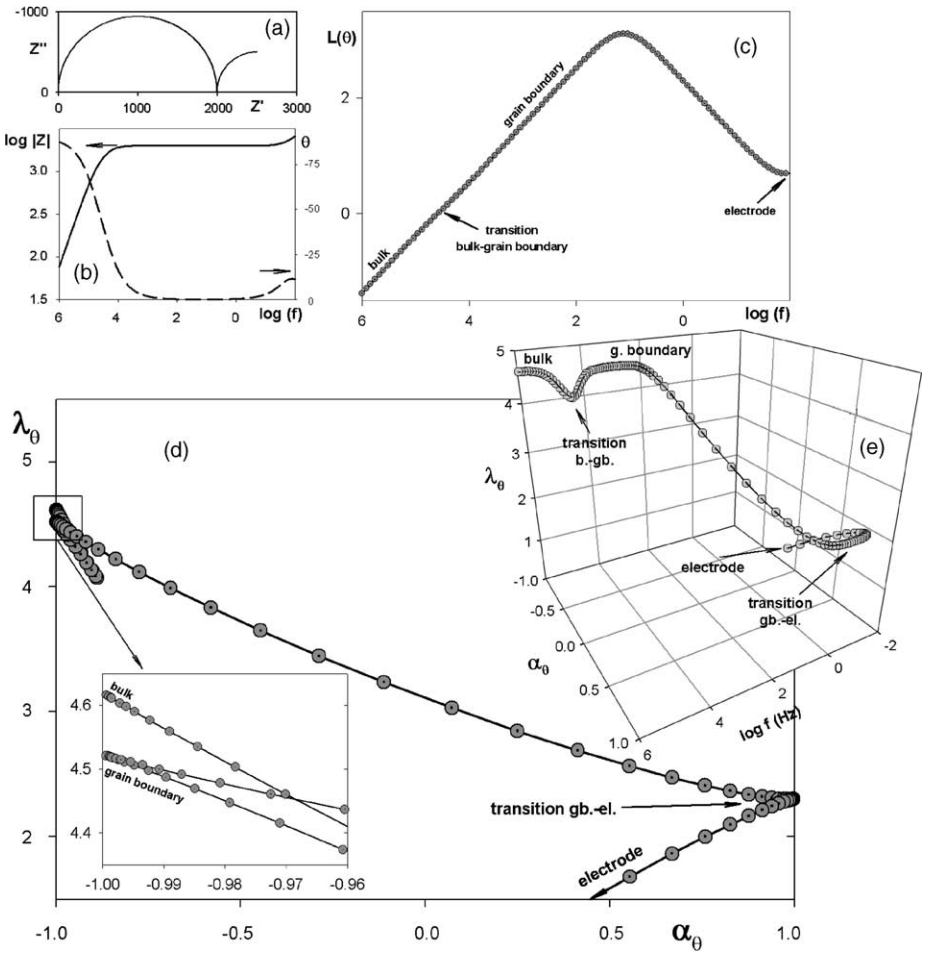

Fig. 6. Impedance spectra computed for $R_b = R_{gb} = R_{el} = 10^3\ \Omega$, $f_b = 5 \times 10^4$ Hz, $f_{gb} = 2.5 \times 10^4$ Hz and $f_{el} = 1 \times 10^{-2}$ Hz. Nyquist plot (a), the corresponding plots of magnitude, $|Z|$ and phase angle, θ, vs. frequency (b), and $L(\theta)$ vs. $\log(f)$ (c), and the new alternative representation of the impedance data in 2D (d) and 3D (e).

On the other hand, the parameter with more imprecision corresponds to the straight line with the slope -1 at low frequency, where the theoretical value is -1.52 and the obtained value is -1.23. The main reason for this discrepancy arises for the narrowness of the linear region, which produces a large inaccuracy in the extrapolation of this line. Further experimental points at lower frequency could improve the accuracy of this extrapolated value.

Actually, the new representation can be very useful if we take the data obtained from this method and set up non-linear least square fitting since it allows us to know the correct number of series element and also provides good initial parameters. With non-linear least-squares (NLLS) it is often difficult to decide upon the correct circuit model and erroneous fitting will ensure. Similarly false minima will be avoided. In addition, this approach will be very valuable where a high degree of correlation is observed in NLLS fitting without constants.

3.4. Case 4, YSZ pellet

As an initial test of this treatment, a dense pellet of 8 mol% Y_2O_3/ZrO_2, YSZ (Tosoh) was prepared. The impedance spectrum was performed at 325 °C (Fig. 7).

From the classic representations of Nyquist (Fig. 7a); or the plots of both magnitude $|Z|$ and phase angle θ versus frequency (Fig. 7b); or the plot of $L(\theta)$ versus $\log(f)$ (Fig. 7c) the same conclusion is reached, that is, it is possible to observe clearly three processes.

With the new alternative representation (Fig. 7d and e), it is also possible to confirm the existence of the three processes: bulk, grain boundary and electrode processes. The corresponding extrapolations and intercepts points allow us to obtain the relationships between the parameters studied (Table 3, case 4).

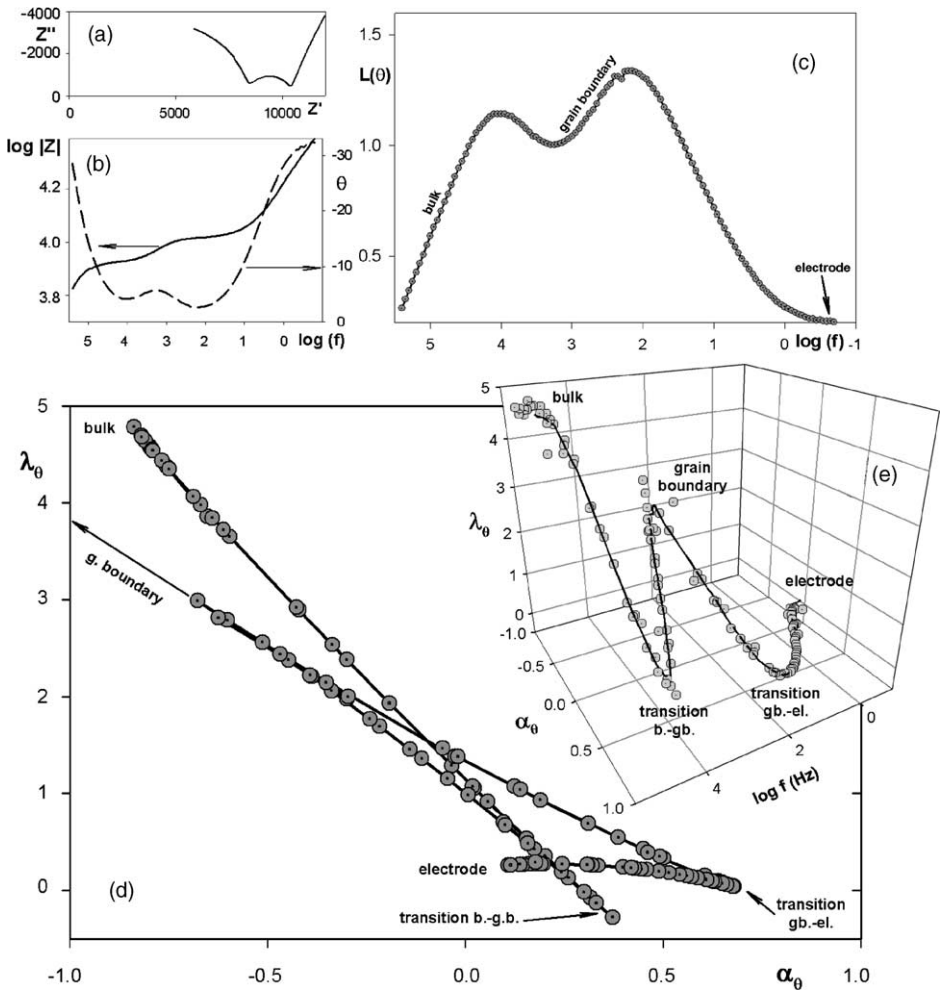

Fig. 7. Impedance spectra obtained for YSZ pellet, at 325 °C, sintered at 1400 °C for 12 h. Nyquist plot (a), the corresponding plots of magnitude, $|Z|$ and phase angle, θ, vs. frequency (b), and $L(\theta)$ vs. $\log(f)$ (c), and the new alternative representation of the impedance data in 2D (d) and 3D (e).

From these values and combining them with the data obtained from the plots of magnitude, |Z|, ($R_b = 8438\ \Omega$ and $R_{gb} = 2005\ \Omega$) it is possible to obtain all the parameters using only some of the proposed equations Eqs. (2)–(4), (6) and (9). Thus, from Eq. (2) the bulk relaxation frequency is directly obtained, $f_b = 3.7 \times 10^5$ Hz. Using this value into Eq. (3) lets us find the grain boundary relaxation frequency, $f_{gb} = 1.4 \times 10^3$ Hz. On the other hand, Eqs. (6) and (9), allow us to obtain a mean value for the relationship $R_{el}f_{el} = 3.1 \times 10^4$. Using this value in Eq. (4) we find an approximate value for the relaxation frequency and resistance of the electrode process, $R_{el} = 3.6 \times 10^4\ \Omega$ and $f_{el} = 0.9$ Hz.

Finally keeping in mind the connection between the relaxation frequencies and the resistances and capacities of each process, the remaining parameters finally are determined: $C_b = 6.5\ \text{pF cm}^{-1}$, $C_{gb} = 7.3\ \text{nF cm}^{-1}$ and $C_{el} = 7.8\ \mu\text{F cm}^{-2}$.

The obtained values allow the remaining parameters to be calculated from the theoretical equations (Table 3, case 4). As can be seen, the agreement between experimental and theoretical data is good,

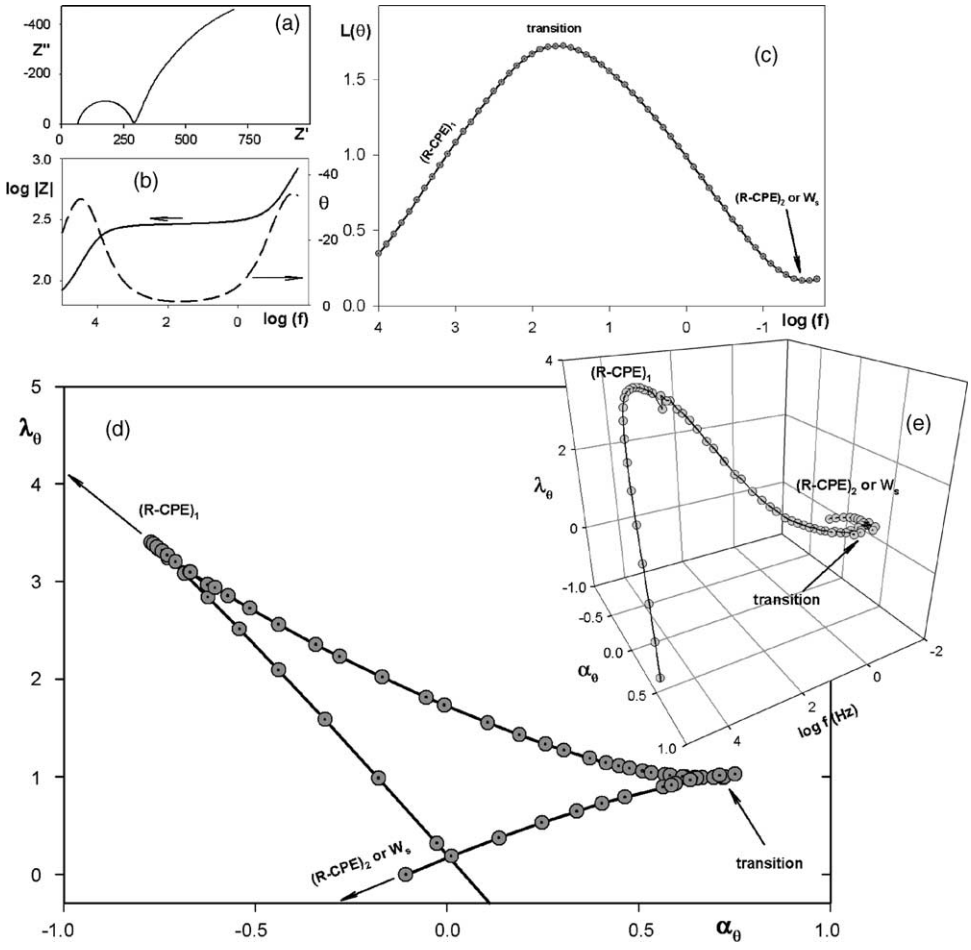

Fig. 8. Impedance spectra obtained for CuO composite (60% CuO + 40% YZTC6), in 5% H_2 (wet), at 500 °C, symmetrical cell. Nyquist plot (a), the corresponding plots of magnitude, |Z| and phase angle, θ, vs. frequency (b), and $L(\theta)$ vs. log(f) (c), and the new alternative representation of the impedance data in 2D (d) and 3D (e).

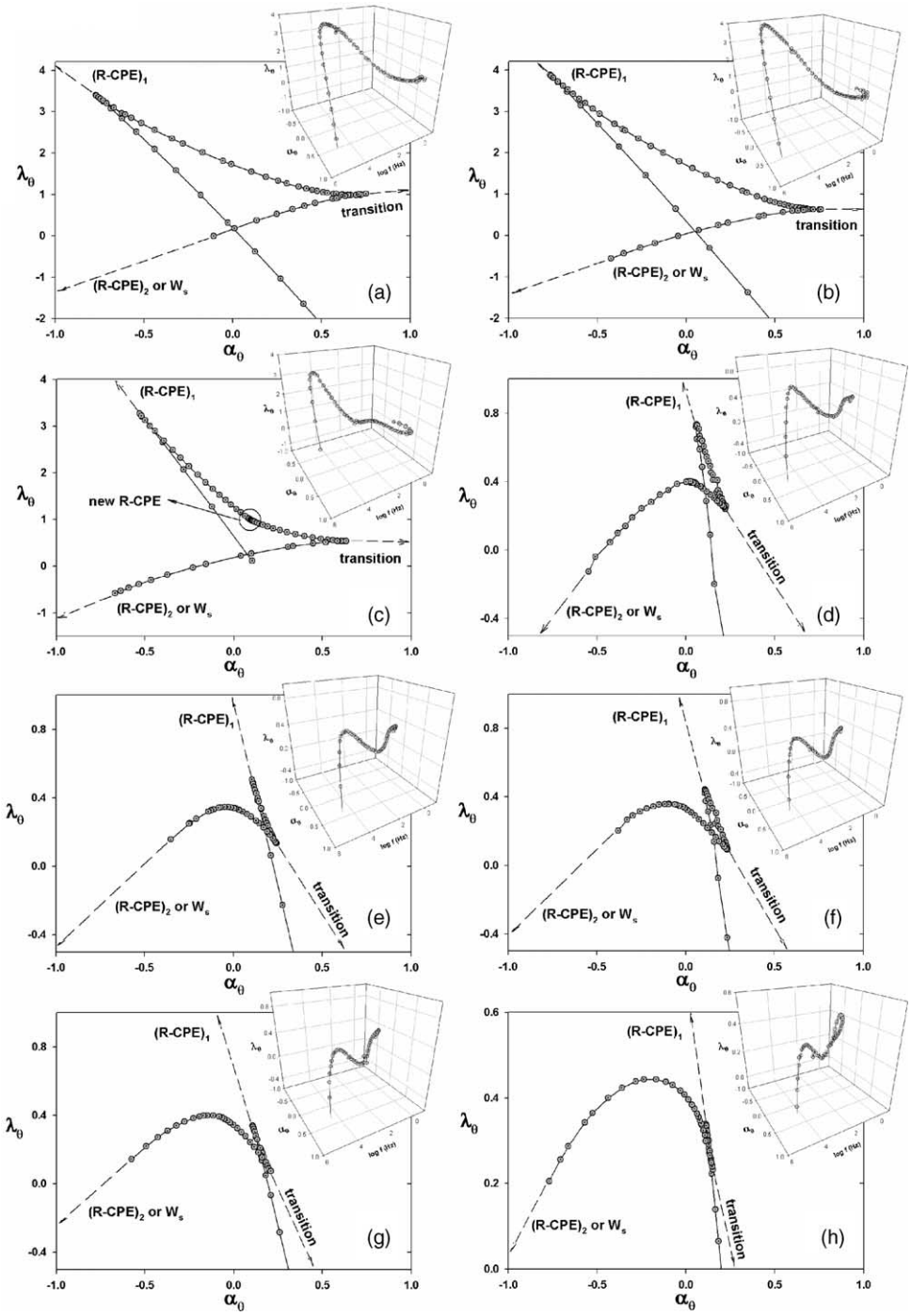

Fig. 9. New alternative representation of the impedance in 2D and 3D plot, for CuO composite (60% CuO + 40% YZTC6), in 5% H_2 (wet), at 500 °C (a), 550 °C (b), 600 °C (c), 650 °C (d), 700 °C (e), 750 °C (f), 800 °C (g), and 900 °C (h).

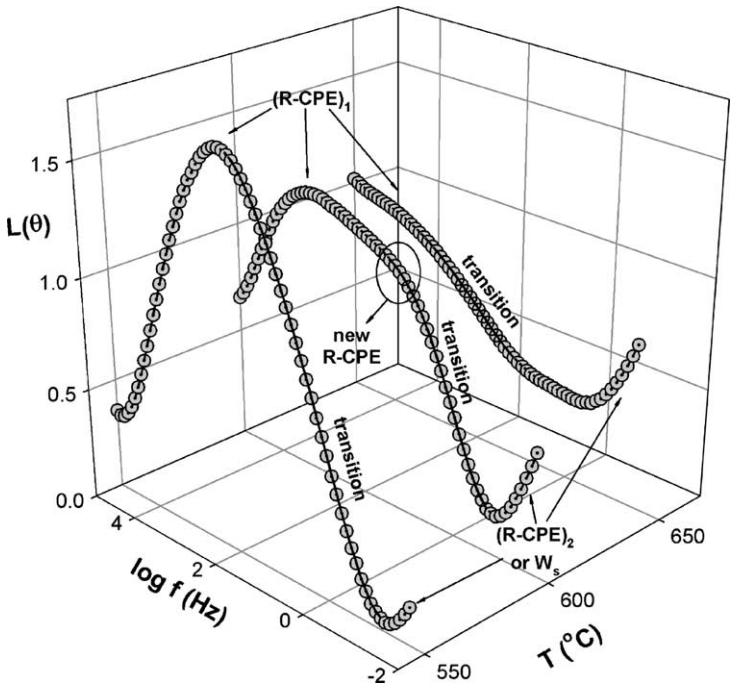

Fig. 10. Plot of $L(\theta)$ vs. log(f) for CuO composite (60% CuO + 40% YZTC6), in 5% H_2 (wet), at 550, 600 and 650 °C.

except for those where the electrode process is involved. The discrepancies do not arise due to the extrapolation method, the origin of the discrepancies comes from the fact that the theoretical development has been outlined for ideal processes; in consequence the existence of non-ideal processes will affect the results. For this reason, if we make a fitting of the experimental data with an equivalent circuit formed by R-CPE elements, instead of RC, it is possible to observe that the exponents of the CPE, for the bulk and the grain boundary, are approximately of 0.9, that which agrees with the values obtained by the new representation. For the electrode process, at lower frequencies, the exponent is about 0.75, so far from the ideal value 1. This explains the discrepancies with the intercepts for this process. The value of this new method in identifying the number of involved processes and initial parameters is clearly demonstrated.

3.5. Case 5, composite electrode, symmetrical cell measurements

In a further example, a CuO composite sample (60% CuO + 40% YZTC6) has been studied. The impedance spectra were obtained from 500 to 900 °C in 50 °C steps. Fig. 8 shows the impedance spectrum for 500 °C.

From the classic representations of Nyquist (Fig. 8a); or the plots of both magnitude |Z| and phase angle θ versus frequency (Fig. 8b); or the plot of $L(\theta)$ versus log(f) (Fig. 8c), we can observe two processes.

With the new alternative representation (Fig. 8d and e), it is possible to confirm the existence of two processes. Independent of the series resistance of the electrolyte and electrode that can be obtained from the high frequency intercept, we have one R-CPE1 element at higher frequencies, and at lower

frequencies we can have another R-CPE2 and a diffusion element, but depending on the impedance values the contribution of one process can be higher than the other.

At 500 °C (Fig. 9a) and 550 °C (Fig. 9b), the shape of the new representation is approximately the same. Nevertheless, at 600 °C (Fig. 9c), something new happens, because it is possible to see a high concentration of points between the first R-CPE element and the transition. However, as can be deducted from the text, the accumulation of points only happens close to a RC element or in the transition zones. Anyway, that it means the existence of another arc or process. From 650 °C (Fig. 9d), the shape changes dramatically and it remains similar until 900 °C (Fig. 9h). Probably this change between 600 and 650 °C is related with microstructural changes. For this system [22], we have observed indications of segregation of Cu from the anode material to the interface between the electrolyte and the anode material at around 650 °C. Similar conclusions can be extracted from the 3D plots. Until 550 °C the shape is similar but at 600 °C we can see a transition around 300 Hz and the plot shape changes dramatically at 700 °C. From this type of plot, it is possible to see very active changes at lower frequencies, usually related with adsorption and diffusion processes for all the temperatures. Fig. 10 shows the dependence of $L(\theta)$ versus $\log(f)$, in the transition between 550 and 650 °C.

4. Conclusions

The usefulness of this new alternative representation of impedance data has been shown. This representation allows us to discriminate rapidly the number of processes in the spectra. Also, all the parameters of these processes can be extracted: relaxation frequencies, resistances and capacities, from this representation or in combination with classic representations, specially, $|Z|$ versus f.

Theoretical equations for the simplified behaviour of the impedance data are proposed. These equations can be directly used to obtain the parameters previously commented or can be included in non-linear fitting software to limit the possible range of variation of the parameters studied. This method can be applied to provide starting parameters for non-linear least squares fitting using constant phase elements, in that case problems due to correlation of parameters and identification of components can be minimised.

Finally, we have demonstrated the high resolution of the new alternative representation that depending on the analysed processes, it can be able to solve overlapped processes within a factor of 2 in their relaxation frequencies, and even qualitative analysis can be achieved with high level of resolution.

Acknowledgements

The authors would like to acknowledge the EPSRC, EU Marie Curie and ESF OSSEP for their financial support for this work.

References

[1] J.R. Macdonald, Impedance Spectroscopy, Wiley-Interscience, New York, 1987.
[2] J.C.C. Abrantes, J.A. Labrincha, J.R. Frade, Mater. Res. Bull. 35 (2000) 955.

[3] J.C.C. Abrantes, J.A. Labrincha, J.R. Frade, Mater. Res. Bull. 35 (2000) 965.
[4] J.T.S. Irvine, D.C. Sinclair, A.R. West, Adv. Mater. 2 (1990) 132.
[5] D.C. Sinclair, A.R. West, J Appl. Phys. 66 (8) (1989) 3850.
[6] H. Schichlein, A. Müller, M. Voigts, A. Krügel, E. Ivers-Tiffée, in: S.C. Singhal, H. Yokokawa (Eds.), Proceeding of 7th International Symposium on Solid Oxide Fuel Cells, PV 2001−2016, The Electrochemical Society, Pennington, NJ, 2001, p. 564.
[7] H. Schichlein, A.C. Müller, M. Voigts, A. Krügel, E. Ivers-Tiffée, J. Appl. Electrochem. 32 (8) (2002) 875.
[8] R.M. Fuoss, J.G. Kirkwood, J. Am. Chem. Soc. 63 (1941) 385.
[9] H.A. Kramers, Z. Phys. 30 (1929) 521.
[10] R.deL. Kronig, J. Opt. Soc. Am. 12 (1926) 547.
[11] J.R. Macdonald, J. Chem. Phys. 102 (15) (1995) 6241.
[12] G. Raikova, Z. Stoynov, D. Vladikova, H. Takenouti, International Workshop on Impedance Spectroscopy for Characterisation of Materials and Structures, P4, Warszawa, Poland, 2003.
[13] J.R. Macdonald, J.A. Garber, J. Electrochem. Soc. 124 (1977) 1022.
[14] J.R. Macdonald, J. Schoonman, A.P. Lehnen, J. Electroanal. Chem. 131 (1982) 77.
[15] J.R. Macdonald, L.D. Potter, Solid State Ionics 24 (1987) 61.
[16] B.A. Boukamp, Solid State Ionics 20 (1986) 31.
[17] B.A. Boukamp, J. Electrochem. Soc. 42 (6) (1995) 1885.
[18] K. Levenberg, Q. Appl. Math. 2 (1944) 164.
[19] D.W. Marquardt, J. Soc. Ind. Appl. Math. 11 (1963) 431.
[20] J.E. Bauerle, J. Phys. Chem. Solids 30 (1969) 2657.
[21] J.G. Fletcher, A.R. West, J.T.S. Irvine, J. Electrochem. Soc. 142 (1995) 2659.
[22] J.C. Ruiz-Morales, P. Núnez, R. Buchanan, J.T.S. Irvine, J. Electrochem. Soc. 150 (8) (2003) 1030.